FIBER TOXICOLOGY

EDITED BY

David B. Warheit

E.I. du Pont de Nemours & Co.

Haskell Laboratory for Toxicology & Industrial Medicine

Newark, Delaware

ACADEMIC PRESS, INC.

A Division of Harcourt Brace & Company

San Diego New York Boston

London Sydney Tokyo Toronto

1993

CHAPTER

4

Mathematical Models of Fiber Deposition in the Lung

C. P. YU AND B. ASGHARIAN

I. Introduction

Deposition of fibers in the respiratory tract is a dynamic process complicated by the sequential branching of the airway passage, the change in the orientation of individual passages, and the behavior of long fibers in this system. Because of the difficulties in generating monodisperse fibers for inhalation studies, experimental measurements of fiber deposition have been limited to animal species using polydisperse fibers to study potential health effects produced by inhaled fibers in the lung. To estimate fiber deposition in the human lung at given fiber dimensions, mathematical models must be utilized. Few mathematical models of fiber deposition have been done to date. Beeckmans (1972) extended the deposition results of spherical particles to fibers by assuming that fibers were randomly oriented in the airways at all times. He showed that the deposition result for fibers could not be derived directly from that for spherical particles by means of an equivalent spherical particle diameter because this diameter differs depending on the deposition mechanism. In Beeckmans' analysis, fiber removal from the nasopharyngeal air stream and interceptional deposition at airway bifurcations were neglected. These losses are significant for large and long fibers.

Another mathematical deposition model of fibers was derived by Harris and Fraser (1976). They assumed that fibers in the airways were

oriented either with their major axes along the flow or randomly in space depending upon the flow condition and the strength of fiber's Brownian rotation. Their model included interceptional deposition at airway bifurcations, as well as impactional and interceptional deposition in the nose.

In general, fibers in the airways are neither parallel to the flow nor randomly orientated. The two models described previously therefore cannot be considered correct. A deposition model that addresses this deficiency has been reported by Asgharian and Yu (1988, 1989a). This chapter presents a brief account of their model and some of the existing and new deposition results calculated from the model.

II. Motion of a Single Fiber in a Tube Flow

The dynamics of a fiber in a fluid flow are more complex than of a spherical particle. Because the mobility of a fiber depends upon the fiber orientation with respect to the air flow, both rotational and translational motion must be considered in determining the trajectory of a fiber under an external force. Consider a horizontal circular tube of radius R and length L in which air flows with a parabolic velocity profile at an average velocity U. We define a coordinate system $\{x_i\}$ fixed on the tube with x_2 along the axis of the tube, x_3 in the vertical direction, and x_1 in the horizontal direction. We also define a moving coordinate system $\{x_i'\}$ fixed on the fiber with the origin o' located at the midpoint of the fiber. We choose x_2' in the direction of x_2, x_1' in the radial direction of the tube, and x_3' perpendicular to both x_1' and x_2' as shown in Fig. 1. The position of the fiber is described by the radial distance of o' from the tube axis, r, and the angle α, which is the projected angle between x_1' and x_1 in the x_1x_3 plane. The orientation of the fiber is described by two Eulerian angles θ and ϕ as shown in the figure.

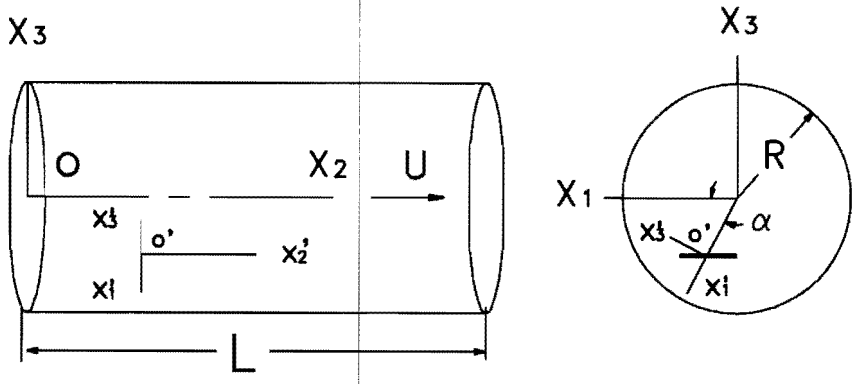

Fig. 1 Duct geometry and coordinate systems.

Neglecting the fiber inertial and the random force and torque on the fiber, the equations of motion for the fiber based upon an ellipsoidal fiber model are given by (Chen and Yu, 1991a)

$$\frac{dx_2}{dt} = 2U\left(1 - \frac{r^2}{R^2}\right), \tag{1}$$

$$\frac{d\theta}{dt} = G\left(\frac{\beta^2 - 1}{\beta^2 + 1}\right)\sin\theta\cos\theta\sin\phi\cos\phi, \tag{2}$$

$$\frac{d\phi}{dt} = G\frac{\beta^2\cos^2\phi + \sin^2\phi}{\beta^2 + 1}, \tag{3}$$

where

$$G = \frac{du}{dr} = -\frac{4Ur}{R^2} \tag{4}$$

is the local velocity gradient of the tube flow, and β is the aspect ratio (length to diameter) of the fiber.

Equations (2) and (3) were solved by Jeffery (1923) and the solutions are

$$\tan\phi = \beta\tan\left(\frac{2\pi t}{T} + C_1\right), \tag{5}$$

$$\tan\theta = \frac{C_2}{\sqrt{\beta^2\cos^2\phi + \sin^2\phi}}, \tag{6}$$

where

$$T = \frac{2\pi(\beta^2 + 1)}{\beta G}, \tag{7}$$

and C_1 and C_2 are two constants related to the initial orientation angles of the fiber θ_0 and ϕ_0. Equations (5) and (6) imply that the fiber undergoes a periodic rotational motion about the x_3' axis. The period of rotation T increases with the aspect ratio β but decreases with the velocity gradient G. Figure 2 shows the trajectory and orientation of a fiber for $\beta = 10$, $x_1(0)/R = 0.5$, $x_2(0)/R = x_3(0)/R = 0$, and $\theta_0 = \phi_0 = 45°$. The complex behavior of fiber orientation in the flow is evident.

III. Orientational Distribution Function

For a system which contains many fibers, the orientation of fibers is described by an orientational distribution function $P(\theta,\phi,t)$ at a given location in space. Because Brownian rotation also contributes to orienta-

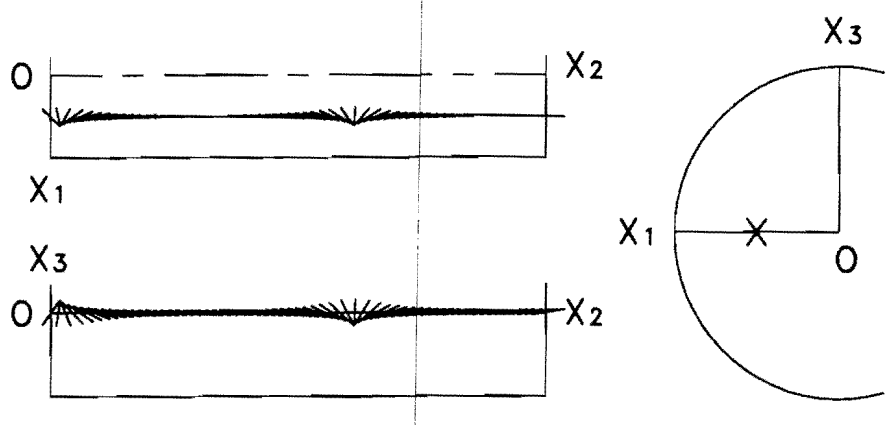

Fig. 2 Trajectory of a fiber in a parabolic flow for $\beta = 10$, $x_1(0)/R = 0.75$, $x_3(0)/R = 0$, $\theta_0 = 45°$, and $\phi_0 = 45°$. The fiber length is exaggerated.

tion for thin fibers, the change of $P(\theta,\phi,t)$ with time is governed by the Fokker–Planck equation

$$\frac{\partial P}{\partial t} + \nabla \cdot (\vec{\omega} P + D_r \nabla P) = 0, \tag{8}$$

where $\vec{\omega}$ is the angular velocity of the flow and D_r is the rotational Brownian diffusion coefficient. The solution of $P(\theta,\phi,t)$ must satisfy the normalized condition

$$\int_0^{2\pi} \int_0^{\pi} P(\theta,\phi,t) \sin\theta d\theta d\phi = 1. \tag{9}$$

For the parabolic flow shown in Fig. 1, $\vec{\omega}$ is in the x_3' direction and has a magnitude of $G = -4Ur/R^2$. At a given r with G constant, Peterlin (1938) found an analytical solution of Eqs. (8) and (9) at the steady state ($t \to \infty$) in the form

$$P(\theta,\phi,t\to\infty) = \frac{1}{2\pi}\left\{1 + \frac{3\Delta \sin^2\theta}{1 + \left(\frac{6}{\mathrm{Pe}_r}\right)^2}\left(-\frac{1}{2}\cos 2\phi + \frac{3}{\mathrm{Pe}_r}\sin 2\phi\right)\right.$$

$$+ \frac{\Delta^2}{1 + \left(\frac{6}{\mathrm{Pe}_r}\right)^2}\left[-\frac{3}{14}(3\cos^3\theta - 1)\right.$$

$$+ \frac{9}{560}(35\cos^4\theta - 30\cos\theta + 3) + \frac{15\sin^4\theta}{16\left(1 + \frac{100}{\mathrm{Pe}_r}\right)}$$

$$\left.\left.\left(\cos 4\phi\left(1 + \frac{60}{\mathrm{Pe}_r^2}\right) - \frac{16}{\mathrm{Pe}_r}\sin 4\phi\right)\right] + \Delta^3[\cdots]\right\}, \tag{10}$$

where

$$\Delta = \frac{\beta^2 - 1}{\beta^2 + 1}, \tag{11}$$

and

$$\mathrm{Pe}_r = \frac{G}{D_r} \tag{12}$$

is the rotational Péclet number that measures the relative contribution of the velocity gradient and Brownian rotation to the fiber orientation. Equation (10) is a series solution of Δ; a rapid convergence of this equation requires $\Delta \ll 1$, which corresponds to small β. For large β, Δ approaches unity and a large number of terms is needed for an accurate evaluation of $P(\theta,\phi,t \to \infty)$.

The rotational diffusion coefficient in Eq. (12) can be expressed in terms of the fiber dimension in the form (Gans, 1928)

$$D_r = \frac{3kT}{2\pi\mu d_f^3(\beta^4 - 1)}\left[\frac{2\beta^2 - 1}{\sqrt{\beta^2 - 1}}\ln(\beta + \sqrt{\beta^2 - 1}) - \beta\right], \tag{13}$$

where $k = 1.38 \times 10^{-23}$ J/°K is the Boltzman constant, T is the absolute temperature in °K, μ is the air viscosity, and d_f is the fiber diameter. It is readily seen from Eqs. (12) and (13) that for very fine fibers (small d_f) D_r is large and $\mathrm{Pe}_r \to 0$. The solution of $P(\theta,\phi,t \to \infty)$ given by Eq. (10) reduces to

$$P(\theta,\phi,t \to \infty) = \frac{1}{2\pi}, \tag{14}$$

which is a uniform or random distribution in space. On the other hand, for large and long fibers, D_r is small, $\mathrm{Pe}_r \to \infty$, and the fiber orientation is governed by the velocity gradient alone. Equation (10) then becomes

$$P(\theta,\phi,t \to \infty) = \frac{1}{2\pi}\left\{1 - \frac{3}{2}\Delta \sin^2\theta \cos 2\phi + \Delta^2\left[-\frac{3}{14}(3\cos^3\theta - 1) + \frac{9}{560}(35\cos^4\theta - 30\cos\theta + 3) + \frac{15}{16}\sin^4\theta\cos 4\phi\right] + \Delta^3[\cdots]\right\}. \tag{15}$$

Using a Monte-Carlo simulation method, Chen and Yu (1991b) have shown that $P(\theta,\phi,t)$ can reach the steady state when $Gt > 20$, although no steady state solution exists for the orientation of a single fiber.

IV. Deposition Efficiency in an Airway

There are four principal mechanisms that cause fiber deposition within the respiratory tract. These are diffusion, sedimentation, impaction, and interception. The relative contribution of these mechanisms to deposition in an airway, however, depends upon the fiber size and flow rate, as well as the dimension and location of this airway in the respiratory tract. For fibers carrying electric charges, deposition can be further caused by the electrostatic image force (Vincent *et al.*, 1981). Recent theoretical studies (Chen and Yu, 1990, 1991c) on the settling of charged fiber by gravity from a duct flow have shown that deposition is enhanced if the charge level of the fiber is high, but a complete deposition theory of charged fibers in the respiratory tract has yet to be worked out. In this chapter, we shall limit our discussion to uncharged fibers.

In the mathematical model of fiber deposition by Asgharian and Yu (1988, 1989a), the expressions for deposition efficiency due to the mechanisms of diffusion, sedimentation, and impaction were obtained from those for spherical particles (Ingham, 1975; Pich, 1972; Chan and Yu, 1981) but modified to account for the fiber orientation effect. Because diffusional and sedimentational deposition take place mainly in small airways where the velocity profile is parabolic, formulae derived for this flow field were used. For diffusion, the efficiency is

$$\eta_d = 1 - 0.819 \exp(-14.63\Lambda) - 0.097 \exp(-89.22\Lambda) - 0.0325 \exp(-228\Lambda) - 0.0509 \exp(-125.9\Lambda^{2/3}), \quad (16)$$

where

$$\Lambda = \frac{L\overline{D}_t}{4U R^2}, \quad (17)$$

in which L and R are, respectively, the airway length and radius, U is the average velocity of the air flow, and $\overline{D}_t$ is the average translational diffusion coefficient of the fiber in the radial direction of the airway over all fiber orientations. $\overline{D}_t$ is related to the value of $D_t(\theta,\phi)$ at a given orientation by the equation

$$\overline{D}_t = \int_{\phi=0}^{2\pi} \int_{\theta=0}^{\pi} D_t(\theta,\phi) P(r,\theta,\phi,t) \sin\theta d\theta d\phi. \quad (18)$$

The result of $\overline{D}_t$ calculated from Eq. (18) is a function of r and t. However, because diffusional deposition takes place near the wall where the air velocity is small, the function $P(r,\theta,\phi,t)$ in Eq. (18) is evaluated at $r = R$ and $t \to \infty$. $\overline{D}_t$ is therefore a constant.

The deposition efficiency of fibers which settle under gravity in a parabolic flow through a horizontal tube is

$$\eta_s = \frac{2}{\pi}(2\varepsilon\sqrt{1-\varepsilon^{2/3}} - \varepsilon^{1/3}\sqrt{1-\varepsilon^{1/3}} + \sin^{-1}\varepsilon^{1/3}), \tag{19}$$

where

$$\varepsilon = \frac{3\bar{u}_g L}{8UR}, \tag{20}$$

in which $\bar{u}_g$ is the average terminal settling velocity of the fiber over all fiber orientations, given by

$$\bar{u}_g = \frac{2}{\pi}\int_{\alpha=0}^{\pi/2}\int_{\phi=0}^{2\pi}\int_{\theta=0}^{\pi} u_g(\theta,\phi,\alpha)P(r,\theta,\phi,t)\sin\theta d\theta d\phi d\alpha, \tag{21}$$

where $u_g(\theta,\phi,\alpha)$ is the terminal settling velocity at a given orientation. Again, in Eq. (21), $P(r,\theta,\phi,t)$ is evaluated at $r = R$ and $t \to \infty$.

For an airway with an inclination angle γ with the horizontal plane, $\bar{u}_g$ in Eq. (20) should be replaced by $\bar{u}_g \cos\gamma$. Thus, in a system of randomly oriented airways, the average efficiency is given by

$$\bar{\eta}_s = \int_{\gamma=0}^{\pi/2}\eta_s(\gamma)\cos\gamma d\gamma. \tag{22}$$

Impactional deposition occurs at bifurcations of the airways. The deposition efficiency is

$$\eta_{imp} = 0.768\overline{St}\theta_b, \tag{23}$$

where θ_b is the bend angle and $\overline{St}$ is the average Stokes number over all fiber orientations and all radial positions of the airway, i.e.,

$$\overline{St} = \frac{1}{R}\int_{r=0}^{R}\int_{\phi_0}^{2\pi}\int_{\theta=0}^{\pi} St(r,\theta,\phi)P(r,\theta,\phi,t)\sin\theta d\theta d\phi dr, \tag{24}$$

in which $St(r,\theta,\phi)$ is the Stokes number at a given orientation and radial location (Yu *et al.*, 1986). In Eq. (24), $P(r,\theta,\phi,t)$ is evaluated at $t = L/U$ because impaction occurs at the bifurcation located at the end of an airway. Impactional deposition results calculated from Eq. (23) were found to agree well with the experimental data of Kahn (1982) in excised calf lungs.

Fibers also deposit at the carina of a bifurcation by direct interception. Asgharian and Yu (1989b) derived the following expression for the efficiency of this deposition

$$\eta_{int} = \int_{\phi=0}^{2\pi}\int_{\theta=0}^{\pi/2} I(\phi,\theta)\sin\theta d\theta d\phi, \tag{25}$$

where

$$I(\phi,\theta) = \frac{8}{\pi R^4}\int_{\Gamma=0}^{\Gamma'}\int_{r=0}^{\frac{l_p \sin(\Gamma-\Omega)}{2\cos\Gamma}} P(r,\theta,\phi,t)r(R^2 - r^2)drd\Gamma + \frac{1}{R^4}\int_{\Gamma=\Gamma'}^{\pi/2}\int_{r=0}^{r'} P(r,\theta,\phi,t)r(R^2 - r^2)drd\Gamma, \tag{26}$$

in which

$$\Gamma' = \cos^{-1}\left(\frac{l_p}{2R}\cos\Omega\right), \tag{27}$$

$$l_p = l_f\sqrt{1 - \sin^2\theta\sin^2\phi}, \tag{28}$$

$$\Omega = \cos^{-1}\left(\frac{l_f}{l_p}\cos\theta\right), \tag{29}$$

$$r' = \frac{l_p\sin(\Gamma' - \Omega)}{2\cos\Gamma'}, \tag{30}$$

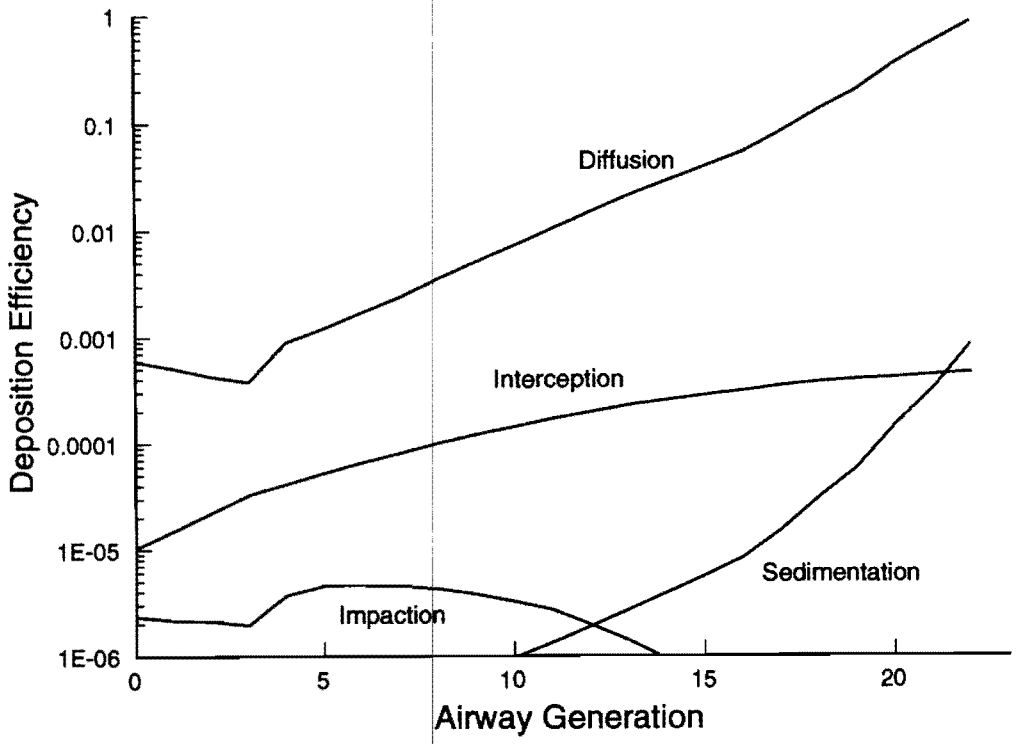

Fig. 3 Deposition efficiency of unit-density fibers in different airway generations of Weibel's lung model at a flow rate of 350 cm^3/sec for $d_f = 0.01$ μm and $\beta = 20$.

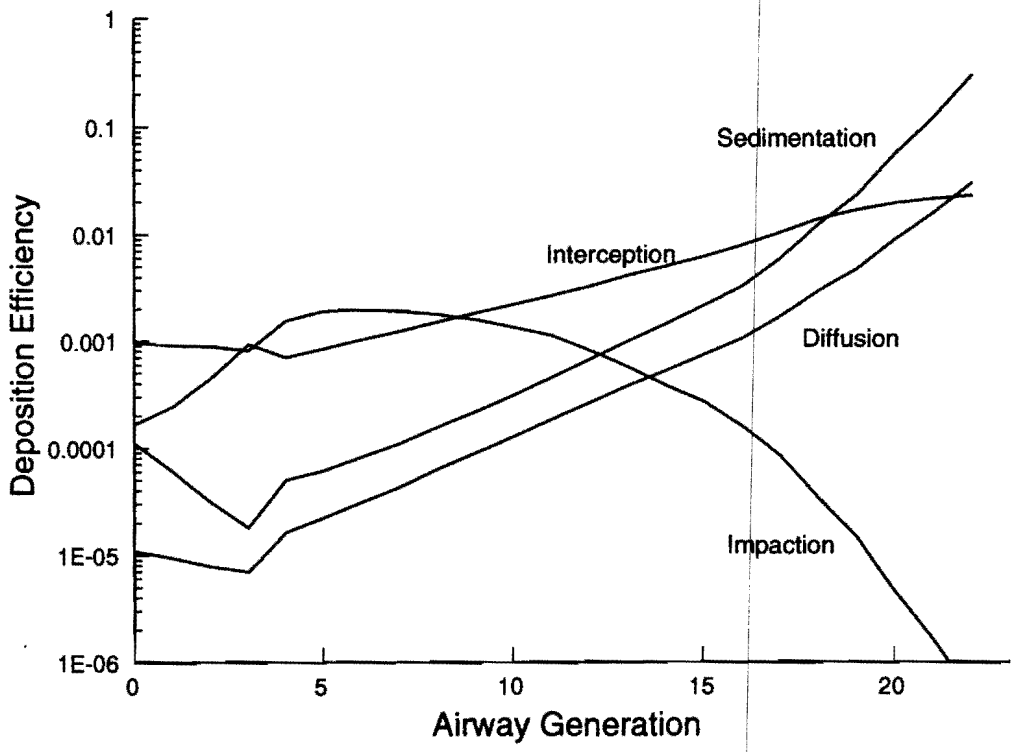

Fig. 4 Deposition efficiency of unit-density fibers in different airway generations of Weibel's lung model at a flow rate of 350 cm^3/sec for $d_f = 0.5$ μm and $\beta = 20$.

and l_f and l_p are, respectively, the fiber length and its projection in the plane of the airway cross section. Similar to the case of impaction, $P(r,\theta,\phi,t)$ in Eq. (26) is evaluated at $t = L/U$.

It is clear from the above derivations that the determination of η_d, $\overline{\eta}_s$, η_{imp}, and η_{int} requires the solution of the orientational distribution function $P(\theta,\phi,t)$ at different r or for different Pe_r. Because the analytical solution of $P(r,\theta,\phi,t)$ is presently not available except for $t \to \infty$ as given by Eq. (10), Asgharian and Yu (1989a) proposed a linear combination solution of η in the following form,

$$\eta = f(Pe_r)\eta_P + g(Pe_r)\eta_R, \tag{31}$$

where

$$f(Pe_r) = \frac{(Pe_r)^b}{a + (Pe_r)^b}, \tag{32}$$

$$g(Pe_r) = \frac{a}{a + (Pe_r)^b}, \tag{33}$$

in which a and b are constants, and η_P and η_R are, respectively, the deposition efficiency for a specific mechanism when the fiber orientation is determined solely by either the velocity gradient or Brownian rotation.

Equation (31) clearly reduces to the correct results of η at two limiting cases of $Pe_r = 0$ and $Pe_r = \infty$. For intermediate Pe_r, it was shown (Asgharian and Yu, 1989b) for the case of interceptional deposition that η calculated from Eq. (31) matched very well with the result obtained by using the series solution of P given by Eq. (10) if constants a and b were chosen to be 50 and 1.5, respectively. Asgharian and Yu (1989b) also showed that the velocity gradient controlled the fiber orientation if $Pe_r > 10^3$, and when $Pe_r < 10^{-2}$, the fiber orientation is random, dominated by Brownian rotation.

Figures 3 to 5 show the calculated results of deposition efficiency by each individual mechanism in different airway generations using Weibel's lung model (1963) and at a flow rate of 350 cm^3/sec for unit density fibers of three different diameters and $\beta = 20$. For very thin fibers ($d_f = 0.01\ \mu m$), Fig. 3 shows that only diffusional deposition is important and its efficiency increases with the generation number because of the increasingly slow flow rate and large residence time. For fibers with $d_f = 0.5\ \mu m$ (Fig. 4), interceptional deposition is the highest from generation 8 to generation 18. Before generation 6, both interception and impaction are important and beyond the 18th generation, sedimentational deposition dominates. For thick fibers ($d_f = 2\ \mu m$) (Fig. 5), impactional deposi-

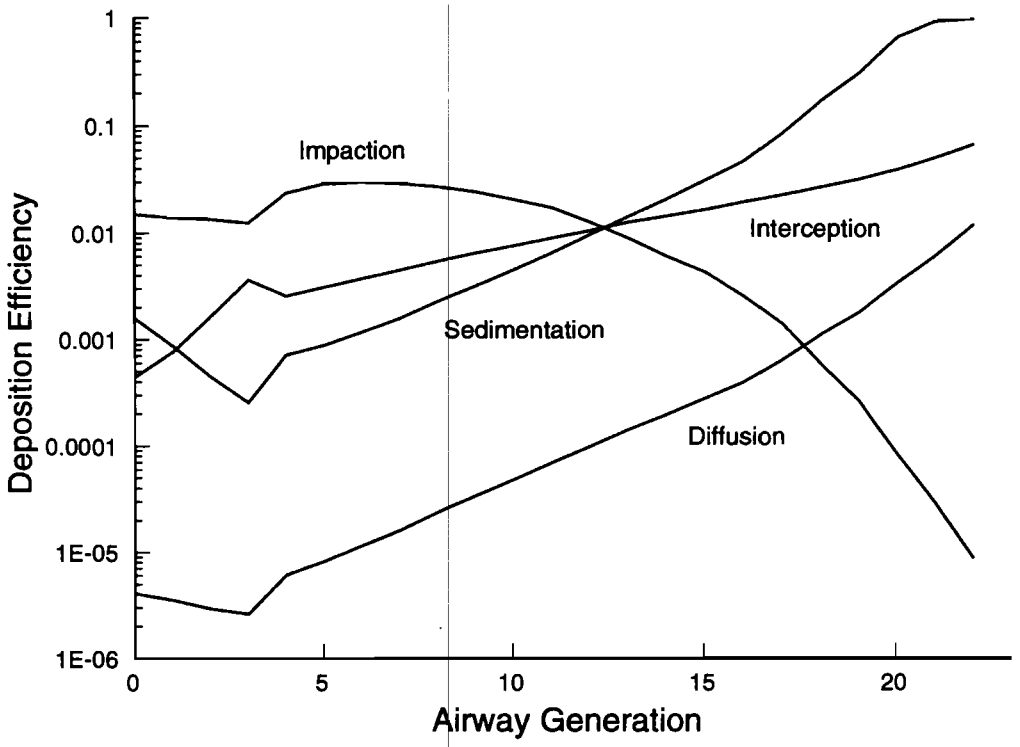

Fig. 5 Deposition efficiency of unit-density fibers in different airway generations of Weibel's lung model at a flow rate of 350 cm^3/sec for $d_f = 2\ \mu m$ and $\beta = 20$.

tion is the highest in the earlier generations of the airways and sedimentational deposition is the highest in later generations, but interceptional deposition plays a significant role in all generations.

V. Deposition Efficiencies in the Nose and Mouth

Fibers also deposit in the head region by impaction and interception. In the mouth, impaction is the only important mechanism, whereas in the nose, interceptional deposition may also occur because of the presence of nasal hairs. The expressions for impactional deposition in the human nose and mouth have been derived by Yu *et al.* (1981) for spherical particles. These expressions were modified for fibers considering the effect of the fiber orientation on the Stokes number in the same manner as Eq. (24). However, due to the high air velocity and complex passages in the head region, fibers were assumed to have a random orientation.

For interceptional deposition by the nasal hairs in the nostril, simple analytical expressions for deposition efficiency were derived by Asgharian (1988). The expressions are

$$N_{\text{int}} = 0.921[1 - (1 - 24l_{\text{f}})^7] \qquad \text{for } l_{\text{f}} < 0.035 \text{ cm}, \tag{34}$$

$$N_{\text{int}} = 0.921 \qquad \text{for } l_{\text{f}} > 0.035 \text{ cm}, \tag{35}$$

where l_{f} is the fiber length in centimeters.

The total collection efficiency in the nose is determined by combining impactional deposition and interceptional deposition. Assuming that these two mechanisms are independent, the total efficiency in the nose N is then

$$N = 1 - (1 - N_{\text{imp}})(1 - N_{\text{int}}) = N_{\text{imp}} + N_{\text{int}} - N_{\text{imp}}N_{\text{int}}, \tag{36}$$

where N_{imp} is the impactional efficiency in the nose. Equations (34) and (35) apply to both inspiration and expiration, but N_{imp} has different expressions for the two processes. At mouth breathing, the total deposition efficiency M is equal to M_{imp}.

Because fiber inhalation experiments have often been conducted in rats, it is useful to compare the deposition results from the calculation with available data. The expressions for deposition efficiency in the airways for rats are the same as those for humans. For impactional deposition efficiency in the rat nose, an empirical equation was derived from the data of Raabe *et al.* (1975) for spherical particles and extended to fibers. The result is

$$N_{\text{imp}} = 0.089 + 0.1158 \log d_{\text{ei}}^2 Q, \tag{37}$$

where Q is the flow rate in cm^3/sec and d_{ei} is the equivalent diameter of the fiber for impaction when the fibers are oriented randomly (Yu *et al.*, 1981). The interceptional deposition by the nasal hairs and impactional deposition through mouth were not considered in the rat model.

VI. Total and Regional Deposition in Rats

Total and regional deposition of fibers in the respiratory tract can be calculated using the formulas for the deposition efficiency presented above using a deposition model for spherical particles such as the one developed by Yu and Diu (1983). In this section, we shall present some calculated deposition results for rats. The lung model employed in the calculation was that of Yeh (1980) but scaled down to a rat lung of 10.78 cm^3, assuming that any linear dimension of the airways was proportional to the cubic root of the lung volume. In addition, the breathing condition consisted of a tidal volume of 1.68 cm^3 and a breathing frequency of 98 breaths per minute, and the breathing cycle consisted of a constant flow inspiratory and a constant flow expiratory process with no pause.

Figures 6–8 show the deposition results in rats for a unit density fiber of different diameters and lengths. The calculation was made for the case where fibers entered the lung via the trachea so there is no nasal deposition. The deposition fraction (the number of fibers deposited divided by the total number of fibers inhaled over a breathing cycle) in the tracheobronchial region, which consists of the first 16 generations of airways, is shown in Fig. 6. It is seen that deposition increases with fiber diameter and length for the fiber size considered but the increase with diameter is much stronger. For thick fibers, deposition in this region is controlled by impaction and interception, whereas thin fibers are deposited by interception only. Figure 7 shows the deposition results in the pulmonary region. Because of the filtration effect in the tracheobronchial region, the dependence of the deposition fraction on the fiber size has a complex pattern in the pulmonary region. The maximum deposition appears to occur at a fiber size with $d_f = 4\ \mu m$ and $l_f = 10\ \mu m$ and is caused principally by the mechanisms of sedimentation and interception. Pulmonary deposition with respect to the fiber size calculated via nose breathing shows a pattern similar to that illustrated in Fig. 7 except that the amount is lower due to the additional filtration effect in the nose. The total deposition result without nasal deposition is shown in Fig. 8.

Experimental data in the rat lung are available for polydisperse fibers. In order to compare the calculated deposition results from the mathematical model with these data, it is necessary to generalize the model to the case of fibers with a size distribution. Airborne fibers normally have a

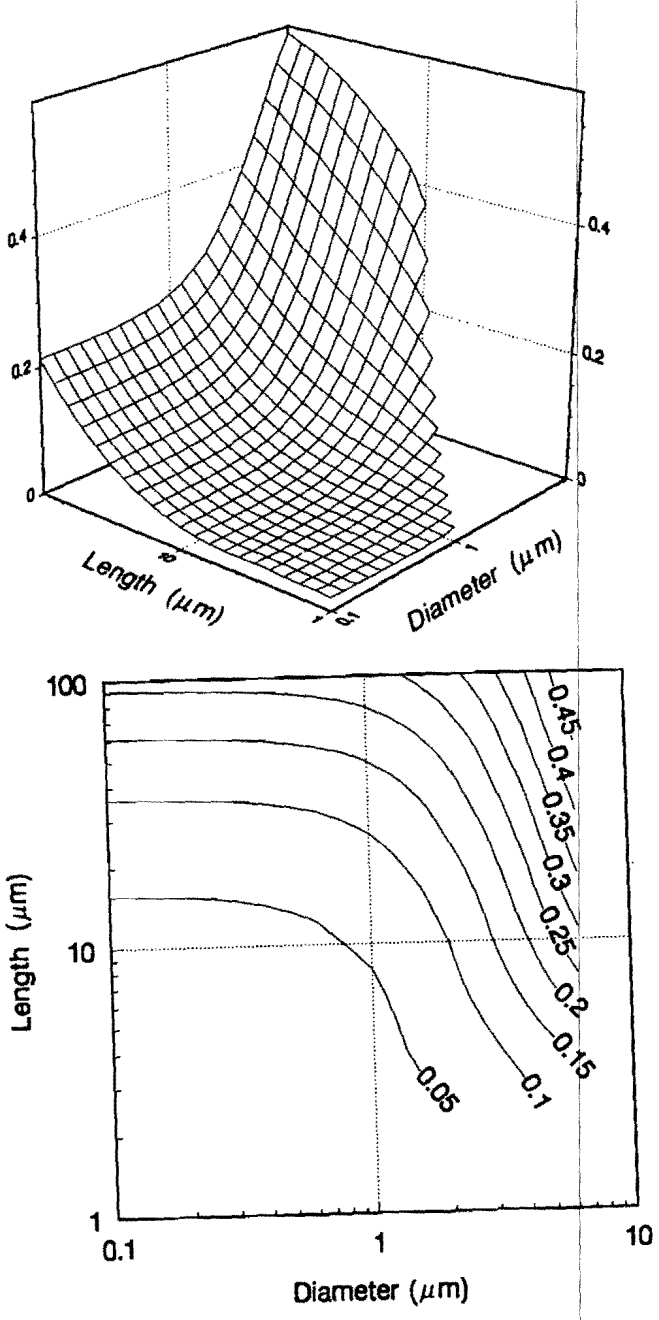

Fig. 6 Deposition fraction of unit-density fibers in the tracheobronchial region of the rat lung for different fiber sizes.

bivariate lognormal distribution in the form (Johnson and Katz, 1972, Cheng, 1986)

$$h(d_f, l_f) = \frac{1}{2\pi \ln \sigma_{gl} \ln \sigma_{gd} \sqrt{1 - \tau^2} l_f d_f} \exp\left[- \frac{A^2 + B^2 - 2\tau AB}{2(1 - \tau^2)} \right], \quad (38)$$

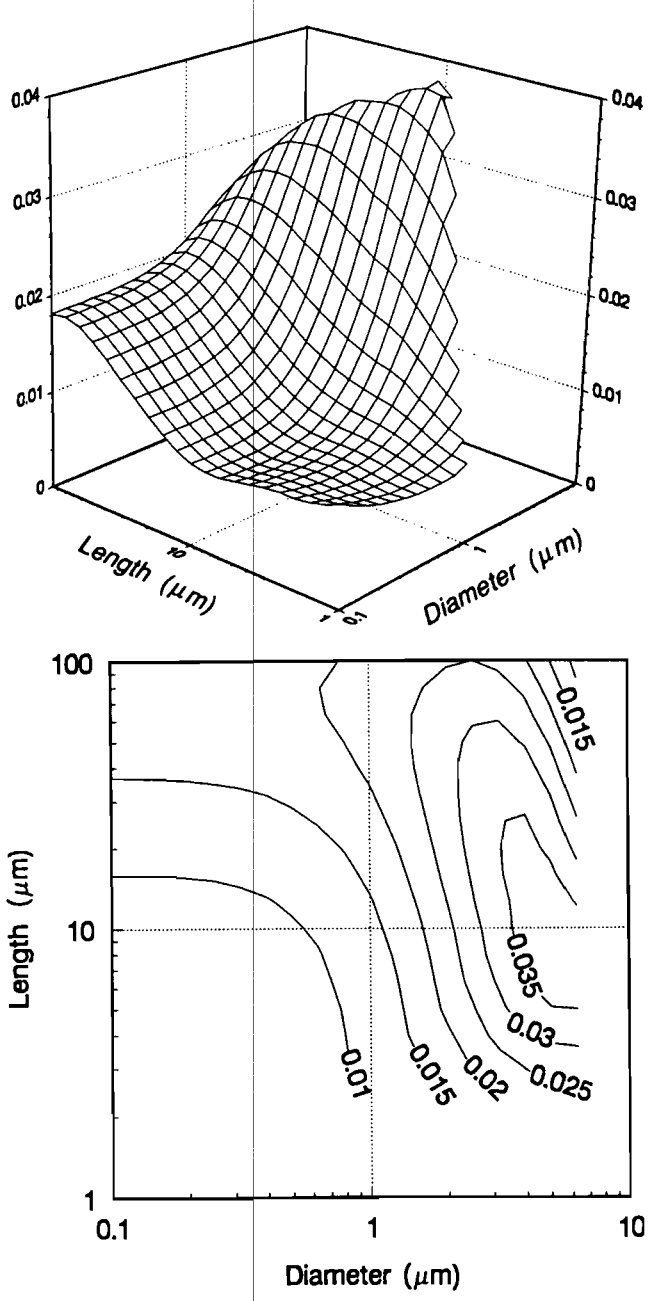

Fig. 7 Deposition fraction of unit-density fibers in the pulmonary region of the rat lung for different fiber sizes.

where

$$A = \frac{\ln d_f - \ln \bar{d}_f}{\ln \sigma_{gd}}, \tag{39}$$

$$B = \frac{\ln l_f - \ln \bar{l}_f}{\ln \sigma_{gl}}, \tag{40}$$

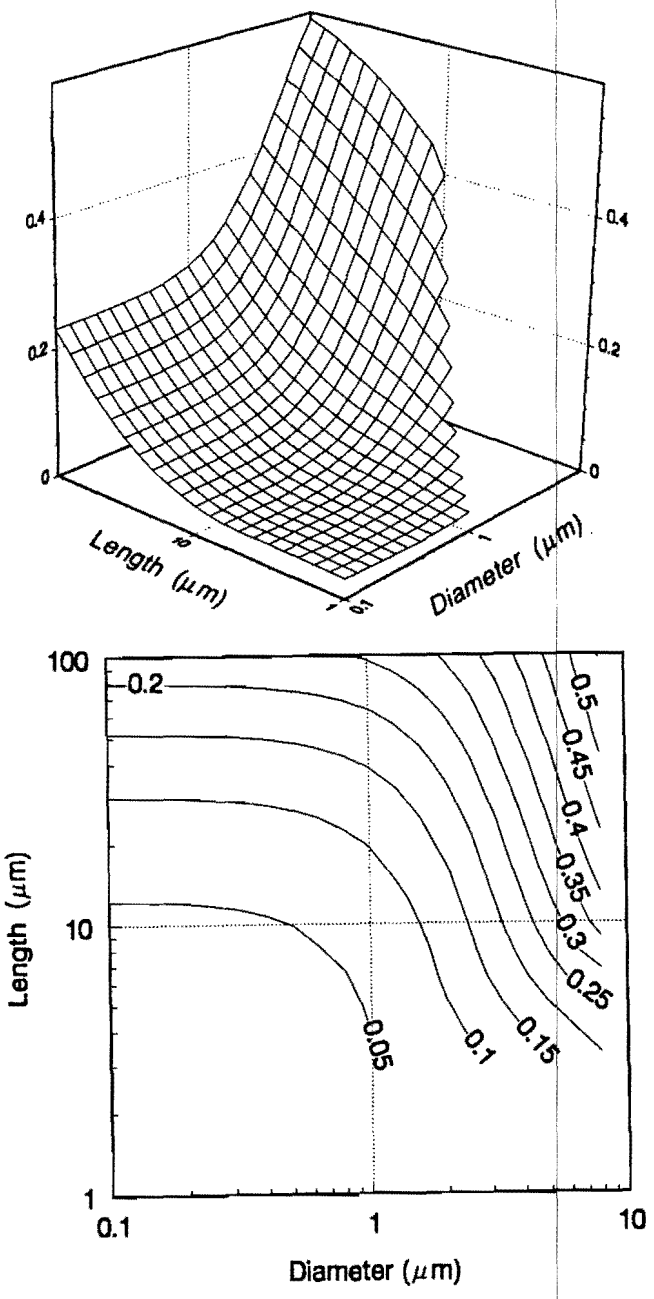

Fig. 8 Total deposition fraction of unit-density fibers in the rat lung for different fiber sizes. Nose deposition is excluded.

in which $\bar{l}_f$ and $\bar{d}_f$ are, respectively, the fiber count median length and diameter, σ_{gl} and σ_{gd} are the corresponding geometric standard deviation, and τ is a length–diameter correlation parameter. Figure 9 shows a fiber distribution with $\bar{d}_f = 0.3$ μm, $\bar{l}_f = 10$ μm, $\sigma_{gd} = 2.26$, $\sigma_{gl} = 2.94$, and $\tau = 0.04$.

The mass fraction deposition of a polydisperse fiber is calculated

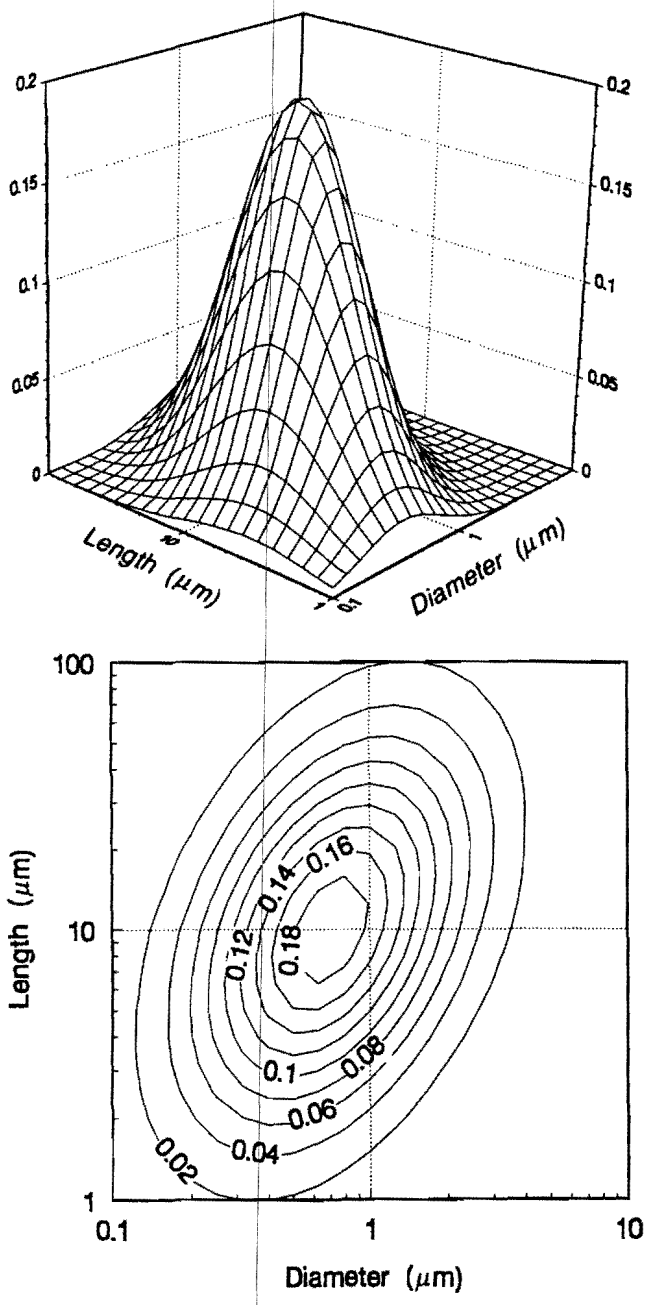

Fig. 9 Bivariate lognormal size distribution of fiber for $\bar{d}_f = 0.3\ \mu m$, $\bar{l}_f = 10\ \mu m$, $\sigma_{gd} = 2.26$, and $\sigma_{gl} = 2.94$.

from the equation

$$DE_m = \frac{\int_0^\infty \int_0^\infty DE(d_f, l_f) d_f^2 l_f h(d_f, l_f) d(d_f) d(l_f)}{\int_0^\infty \int_0^\infty d_f^2 l_f h(d_f, l_f) d(d_f) d(l_f)}, \tag{41}$$

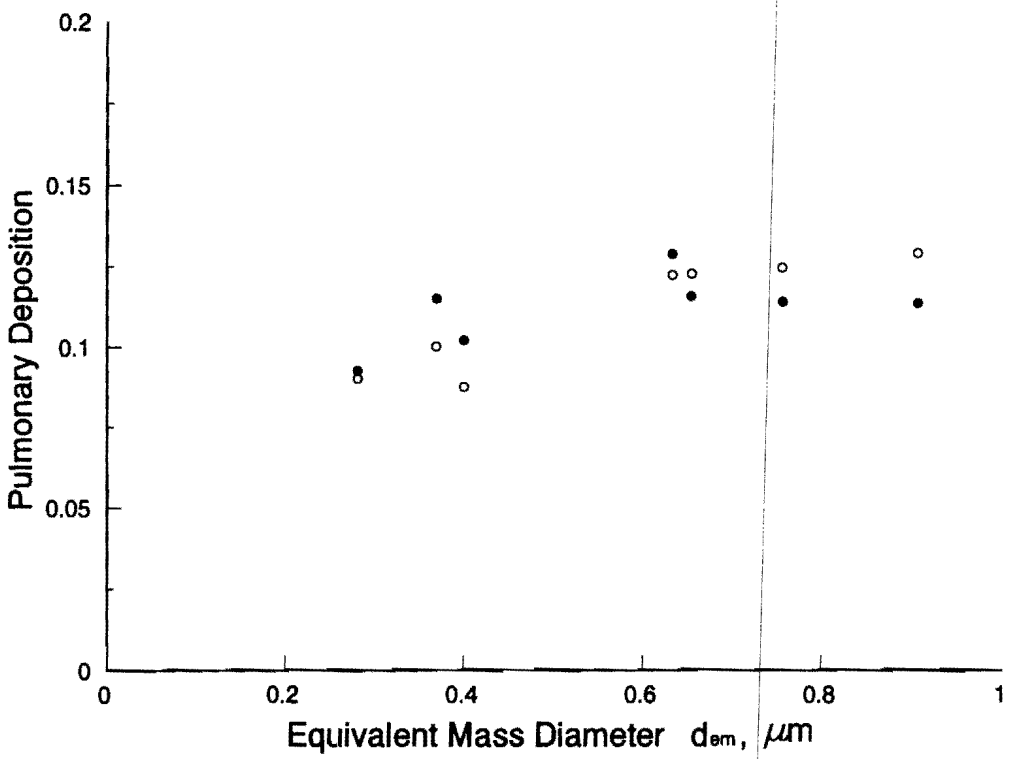

Fig. 10 Comparison of the calculated pulmonary deposition (open circles) in the rat lung with the data (closed circles) of Morgan *et al.* (1977).

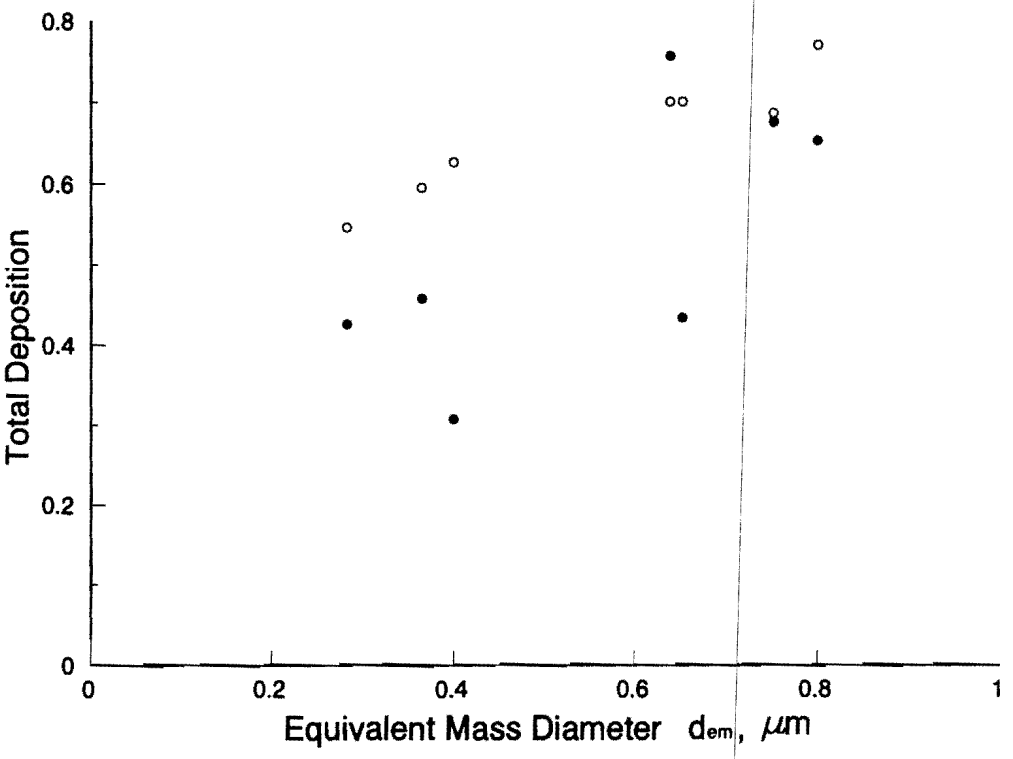

Fig. 11 Comparison of the calculated total deposition (open circles) in the rat lung with the data (closed circles) of Morgan *et al.* (1977).

where $DE(d_f, l_f)$ is the number deposition fraction of a monodisperse fiber of size d_f and l_f. Morgan *et al.* (1977) have measured the mass deposition fraction of seven different asbestos fibers in the rat lung with $\bar{d}_f$ in the range from 0.19 to 0.46 μm, $\bar{l}_f$ from 1 to 5 μm, σ_{gd} from 1.9 to 3 and σ_{gl} from 2 to 2.7. The value of τ was not given. Figures 10 and 11 show, respectively, their data of pulmonary and total deposition through the

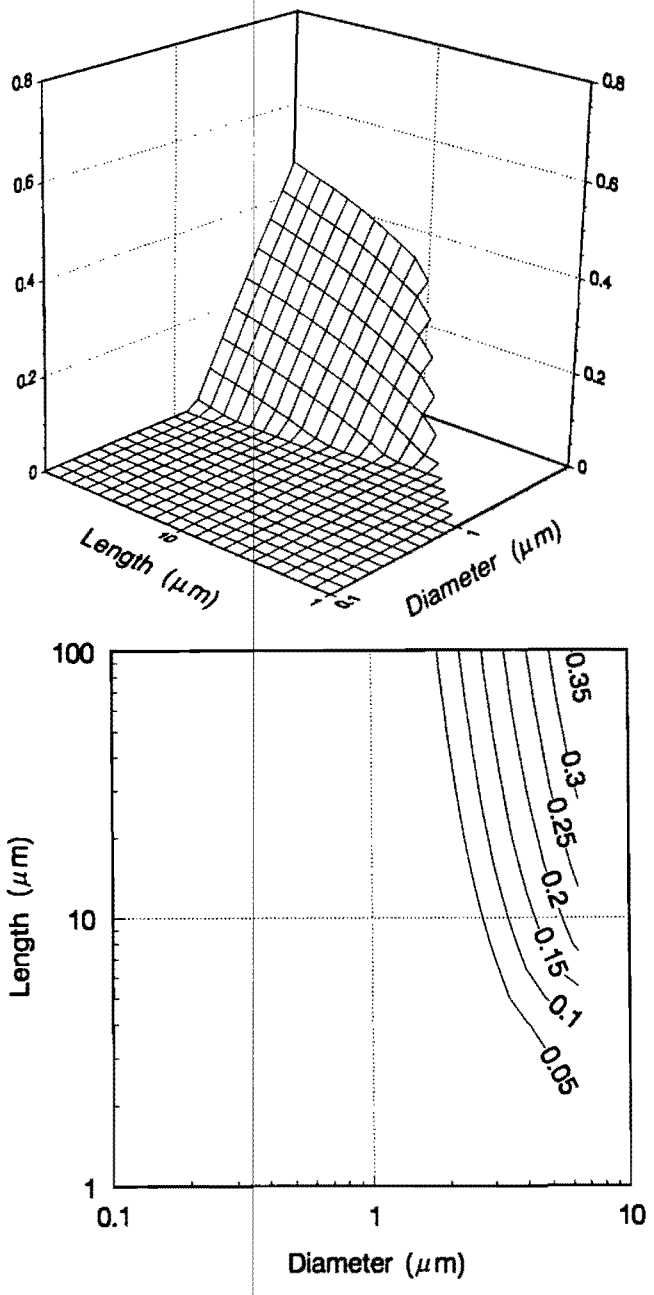

Fig. 12 Deposition fraction of unit-density fibers in the human mouth for different fiber sizes.

nose versus the equivalent mass median diameter $\bar{d}_{em}$ of the fiber, defined by

$$\bar{d}_{em} = \int_0^\infty \int_0^\infty (\rho d_f^2 l_f)^{1/3} h(d_f, l_f) d(d_f) d(l_f), \tag{42}$$

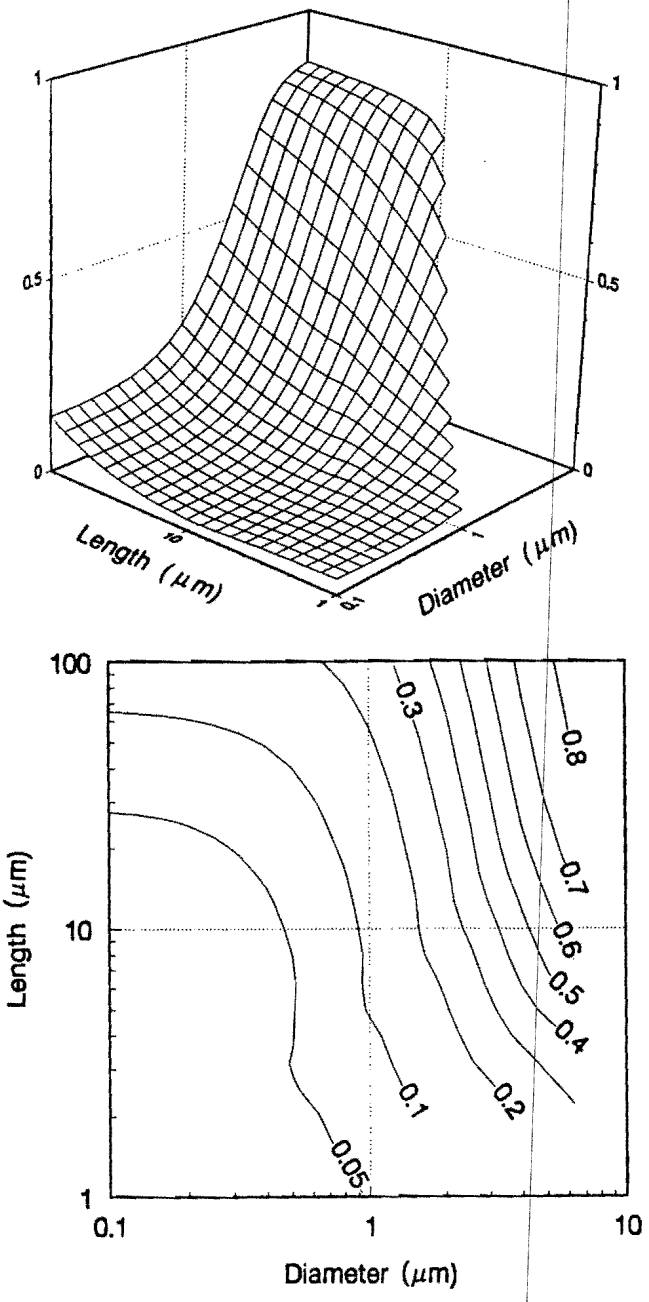

Fig. 13 Deposition fraction of unit-density fibers in the tracheobronchial region of the human lung for different fiber sizes.

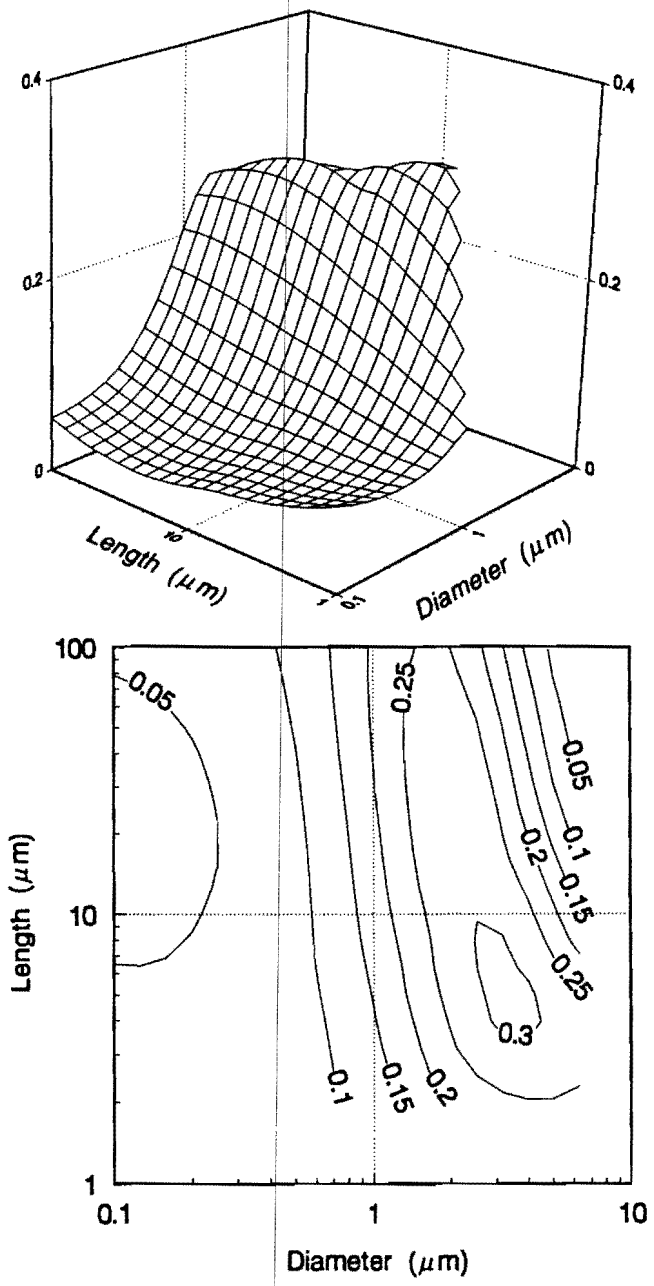

Fig. 14 Deposition fraction of unit-density fibers in the pulmonary region of the human lung for different fiber sizes.

where ρ is the specific mass of the fiber. For comparison, the calculated results from Eq. (41) are also shown in Figs. 10 and 11. The calculations are for $\rho = 3.37$, $\sigma_{gd} = \sigma_{gl} = 2$, $\tau = 0$, and different $\bar{d}_f$ and $\bar{l}_f$. It is seen that calculated deposition fractions agree reasonably well with the data, and for this fiber size range, total deposition increases with $\bar{d}_{em}$ while the pulmonary deposition remains nearly constant.

VII. Total and Regional Deposition in Humans

Total and regional deposition fractions at mouth breathing calculated for unit density fibers of different diameters and length in humans are

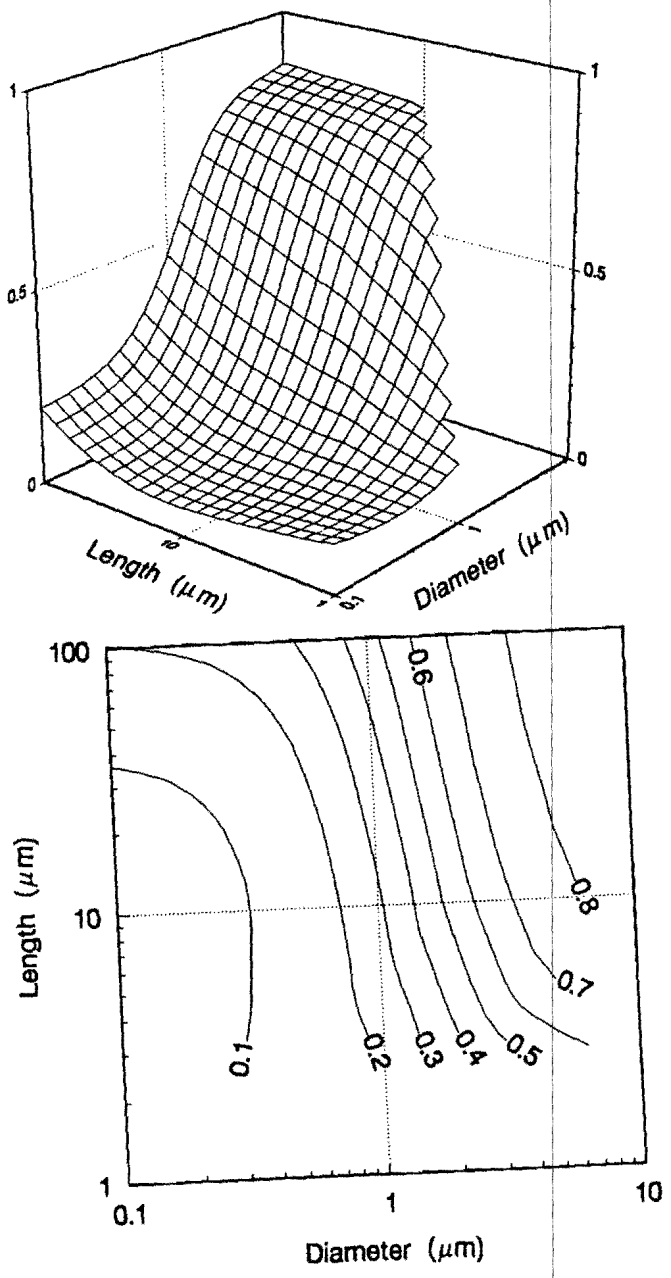

Fig. 15 Total deposition fraction of unit-density fibers via mouth breathing for different fiber sizes.

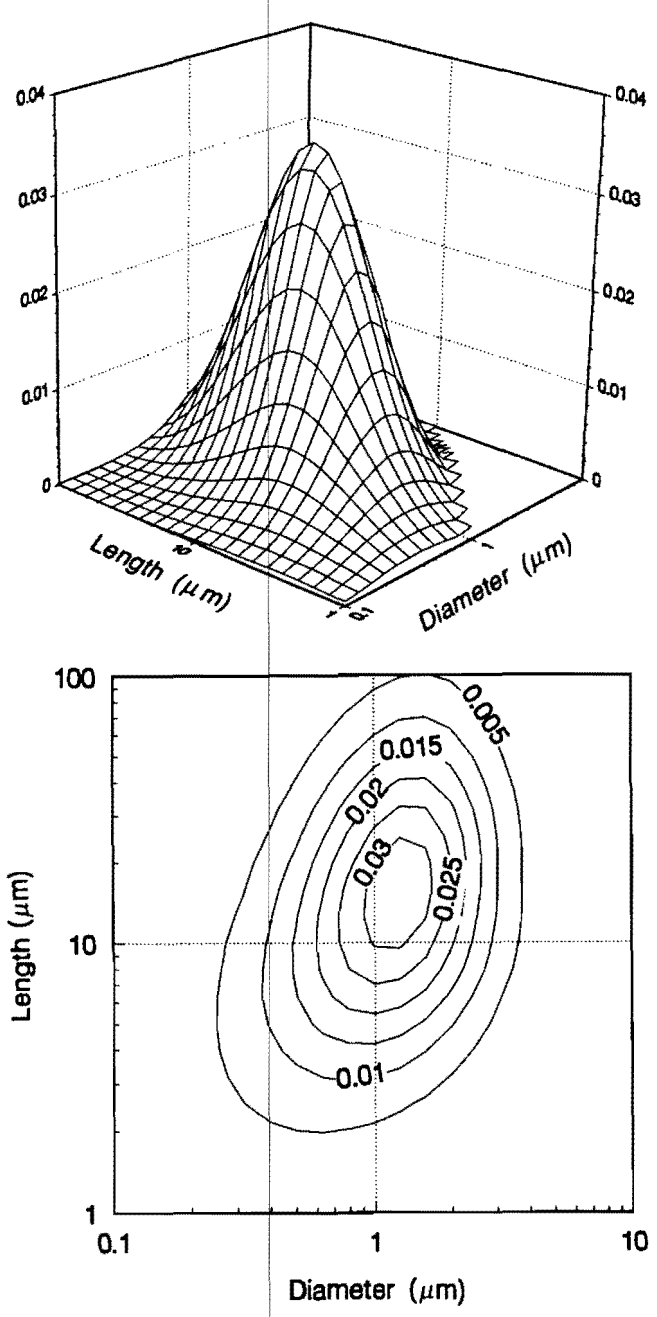

Fig. 16 Pulmonary deposition pattern of unit-density fibers in the rat lung for the fiber size distribution shown in Fig. 9.

shown in Figs. 12–15. The lung model used was Weibel's model (1963) but scaled down to a rest volume of 3000 cm^3. The breathing condition was 500 cm^3 tidal volume and 14 breaths per minute, and the breathing pattern consisted of a constant flow inspiration, a pause, and a constant flow expiration with the respective time fractions equal to 0.435, 0.05, and 0.515 of a breathing period (Task Group, 1966). It is seen that in

the mouth and tracheobronchial regions (Figs. 12 and 13), deposition increases rapidly with diameter for diameters greater than 1 μm. The dependence on the fiber length is relatively weak. This is similar to the tracheobronchial deposition in the rats shown in Fig. 6. However, the dependence of deposition on the fiber length is greater for rats due to higher interceptional deposition. At the same fiber size, Figs. 6 and 13

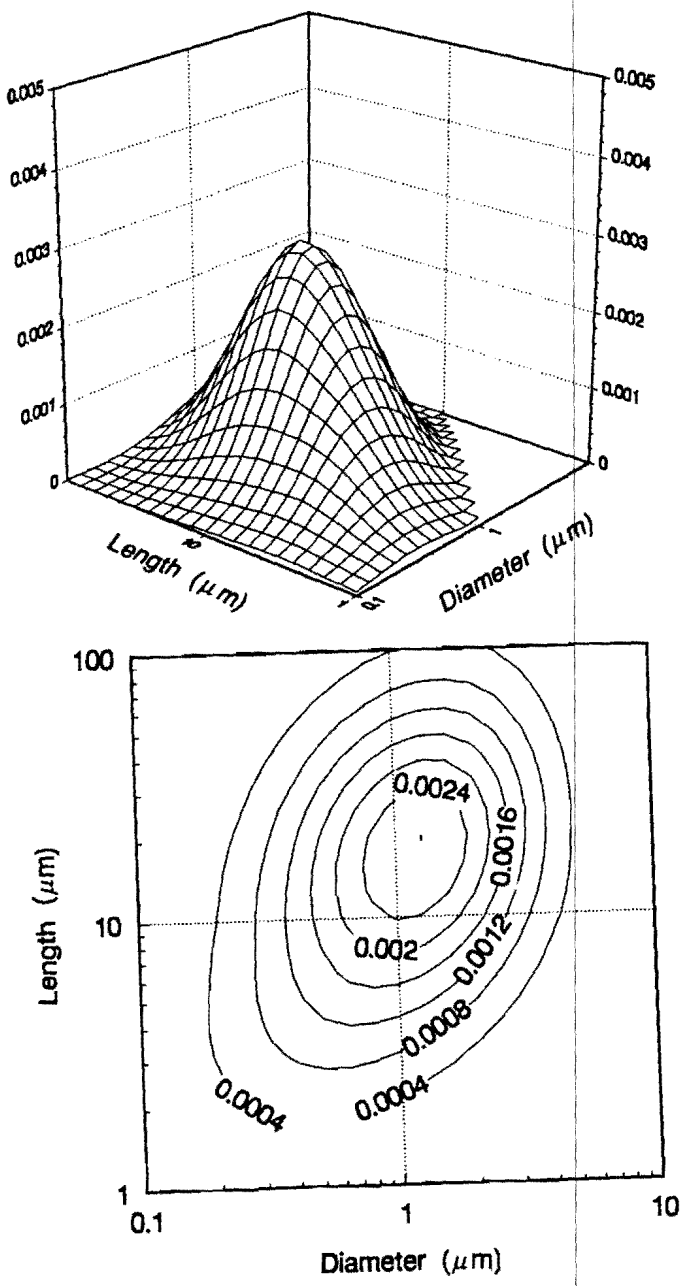

Fig. 17 Pulmonary deposition pattern of unit-density fibers in the human lung for the fiber size distribution shown in Fig. 9.

show that the tracheobronchial deposition in humans is almost twice that of rats. In the pulmonary region, Fig. 14 shows that the deposition fraction in humans is the highest near $d_f = 2$ μm and $l_f = 5$ μm. The magnitude of deposition was found to be 3 to 10 times of that in rats (Fig. 7). Total deposition result in humans at mouth breathing is shown in Fig. 15.

Another interesting comparison of the pulmonary deposition pattern between humans and rats is shown in Figs. 16 and 17 for the inhalation through the trachea of unit density fibers with a size distribution shown in Fig. 9. Despite large differences in the lung structure, the deposition patterns of these two species with respsect to the fiber size were found to be quite similar even though the magnitude in humans is about 10 times higher.

Since no direct deposition data of fibers in the human lung is available, Asgharian and Yu (1988) have compared the calculated deposition results from the mathematical model with the postmortem data of fiber distribution reported by Timbrell (1982) from lung specimen of former employees and local inhabitants of the Paakkila anthophyllite mine in Finland. Timbrell's data represent the fiber retention in the lung after a long period of exposure and thus include the effect of both deposition and clearance. The calculated results of deposition compare very well with these data.

VIII. Concluding Remarks

Motion of a fiber in the airways is a complex dynamic process because the drag force on the fiber varies with the fiber orientation, which constantly changes in the flow. The determination of deposition efficiency in this situation is therefore very complicated. A few mathematical models have been reported in the literature to simulate the deposition process of fibers in the respiratory tract. Although recent models appear to be adequate in explaining existing experimental data, further studies are needed in many specific areas. For example, if secondary flows occur at airway bifurcations, how would such flows affect the orientation and deposition of a fiber? Also, fibers such as asbestos do not have the geometry of a straight cylinder or a long ellipsoid. It is important to know how a fiber which deviates from this idealized geometry would deposit.

Any mathematical model has to be verified by experimental data. Well-controlled deposition experiments in physical models and airway casts are particularly useful to the derivation of deposition efficiency in an airway. Several experimental studies have recently been conducted in large airways using polydisperse fiber (Kahn, 1982; Myojo, 1987, 1990;

Sussman, 1988). However, further data for different airway structures and sizes at different flow rates using monodisperse fibers are critically needed.

Acknowledgments

This work was supported by Grant HL-38803 from the National Heart, Lung, and Blood Institute. We are grateful to Y. K. Chen and L. Zhang for carrying out several calculations.

References

Asgharian, B. (1988). "Theoretical Deposition of Fibrous Particles in the Respiratory System of Humans and Rats." Ph.D. dissertation. Department of Mechanical and Aerospace Engineering, State University of New York at Buffalo.

Asgharian, B., and Yu, C. P. (1988). Deposition of inhaled fibrous particles in the human lung, *J. Aerosol Mec.* **1,** 37–50.

Asgharian, B., and Yu, C. P. (1989a). Deposition of fibers in the rat lung. *J. Aerosol Sci.* **20,** 355–366.

Asgharian, B., and Yu, C. P. (1989b). A simple model of interceptional deposition of fibers at airway bifurcations. *Aerosol Sci. Technol.* **11,** 80–88.

Beeckmans, J. M. (1972). Deposition of ellipsoidal particle in the human respiratory tract. *In* "Assessment of Airborne Particles" (T. T. Mercer, P. E. Morrow, and W. Stober, Eds.). Thomas, Springfield, Illinois.

Chan, T. L., and Yu, C. P. (1981). Charge effect on particle deposition in the human tracheobronchial tree. *Ann. Occup. Hyg.* **33,** 65–75.

Chen, Y. K., and Yu, C. P. (1990). Sedimentation of charged fibers from a two-dimensional channel flow. *Aerosol Sci. Technol.* **12,** 786–792.

Chen, Y. K., and Yu, C. P. (1991a). Sedimentation of fibers from laminar flows in a horizontal circular duct. *Aerosol Sci. Technol.* **14,** 343–347.

Chen, Y. K., and Yu, C. P. (1991b). "Monte-Carlo Simulation of Fiber Orientation in a Shear Flow with Brownian Rotation." Presented at the 1991 American Association for Aerosol Research Meeting, Traverse City, Michigan.

Chen, Y. K., and Yu, C. P. (1991c). Sedimentation of charged fibers from a circular duct flow. *J. Aerosol Sci.* **6,** 747–756.

Cheng, Y.-S. (1986). Bivariate lognormal distributions for characterizing asbestos fiber aerosols. *Aerosol Sci. Technol.* **5,** 359–368.

Gans, K. R. (1928). Zur Theories der Brownschen Moleulargewegung. *Ann. Phys.* **86,** 628–656.

Harris, R. L., and Fraser, D. A. (1976). A model for deposition of fibers in the human respiratory system. *Am. Ind. Hyg. Assoc. J.* **37,** 73–89.

Ingham, D. B. (1975). Diffusion of aerosols from a stream flowing through a cylindrical tube. *J. Aerosol Sci.* **6,** 123–132.

Jeffery, G. B. (1923). The motion of ellipsoidal particles immersed in a viscous fluid. *Proc. R. Sci. A* **102,** 161–179.

Johnson, N. L., and Katz, S. (1972). "Distribution in Statistic: Continuous Multivariate Distributions." Wiley, New York.

Kahn, S. A. (1982). "A Method for Investigation of Deposition of Fibers and Spheres at the Carina in Excised Lungs." Ph.D. dissertation. University of Pittsburgh.

Morgan, A., Evans, J. C., and Holmans, A. (1977). Deposition and clearance of inhaled fibrous minerals in the rat: Studies using radioactive tracer techniques. *In* "Inhaled Particle" (W. H. Walton, Ed.), Vol. IV. Pergamon, Oxford.

Myojo, T. (1987). Deposition of fibrous aerosol in model bifurcating tubes. *J. Aerosol Sci.* **18,** 337–347.

Myojo, T. (1990). The effect of length and diameter on deposition of fibrous aerosol in model lung bifurcation. *J. Aerosol Sci.* **21,** 651–660.

Peterlin, A. (1938). Über die Viskosität von verdünnten Lösungen und Suspensioned in Abhängigkeit von der Teilchenform. *Z. Phys.* **111,** 232–263.

Pich, J. (1972). Theories of gravitational deposition of particles from laminar flows in channel. *J. Aerosol Sci.* **3,** 351–361.

Raabe, O. G., Yeh, H. C., George, J. N., Phalen, R. F., and Velasqucz, D. J. (1975). Deposition of inhaled monodisperse aerosols in small rodents. *In* "Inhaled Particles" (W. H. Walton, Ed.), Vol. IV. Pergamon, Oxford.

Sussman, R. G. (1988). "The Effect of Fiber Dimension on the Deposition of Asbestos Fibers in Casts of the Human Tracheobronchial Tree." Ph.D. dissertation. Institute of Environmental Medicine, New York University, New York.

Task Group on Lung Dynamics (1988). Deposition models for internal dosimetry of the human respiratory tract. *Health Phys.* **12,** 173–207.

Timbrell, V. (1982). Deposition and retention of fibers in the human lung. *Ann. Occup. Hyg.* **26,** 347–369.

Vincent, J. H., Johnston, W. B., Jones, A. D., and Johnston, A. M. (1981). Static electrification of airborne asbestos: A study of its causes, assessment and effects on deposition in the lungs of rats. *Am. Ind. Hyg. Assoc. J.* **42,** 711–721.

Weibel, E. R. (1963). "Morphometry of the Human Lung." Academic Press, New York.

Yeh, H. C. (1980). "Respiratory Tract Deposition Models (Final Report)." Inhalation Toxicology Research Institute, Lovelace Biomedical and Environmental Research Institute, Albuquerque, New Mexico.

Yu, C. P., Diu, C.K., and Soong, T. T. (1981). Statistical analysis of aerosol deposition in nose and mouth. *Am. Ind. Hyg. Assoc. J.* **42,** 726–773.

Yu, C. P., and Diu, C. K. (1983). Total and regional deposition of inhaled aerosols in humans. *J. Aerosol Sci.* **14,** 599–609.

Yu, C. P., Asgharian, B., and Yen, B. M. (1986). Impaction and sedimentation deposition of fibers in airways. *Am. Ind. Hyg. Assoc. J.* **47,** 72–77.